Probing Fano resonances with ultrashort pulses

2012 New J. Phys. 14 065003

(http://iopscience.iop.org/1367-2630/14/6/065003)

New Journal of Physics
The open-access journal for physics

Probing Fano resonances with ultrashort pulses

Jing Zhao[1,2] **and Manfred Lein**[1]

[1] Institut für Theoretische Physik and Centre for Quantum Engineering and Space-Time Research (QUEST), Leibniz Universität Hannover, Appelstraße 2, D-30167 Hannover, Germany
[2] Department of Physics, National University of Defense Technology, Changsha 410073, China

New Journal of Physics **14** (2012) 065003 (11pp)
Received 20 February 2012
Published 1 June 2012
Online at http://www.njp.org/
doi:10.1088/1367-2630/14/6/065003

Abstract. In this paper, autoionizing states in the one-dimensional helium atom are investigated by numerical solution of the time-dependent two-electron Schrödinger equation. The atom is irradiated by an extreme ultraviolet (XUV) attosecond pulse and a time-delayed infrared few-cycle laser pulse. The XUV pulse populates a superposition of doubly excited states, leading to Fano resonances in the photoelectron spectrum. It is demonstrated that the Fano line profile is strongly modified by the presence of the laser field. Laser-induced coupling between the different doubly excited states causes the population of autoionizing states that cannot be reached by absorbing a single XUV photon from the ground state. The resulting additional peaks in the photoelectron spectrum are modulated as a function of time delay. Furthermore, the photoelectron spectrum exhibits a fringe pattern that is determined by the time delay but is independent of the details of the laser pulse.

Contents

1. Introduction

With the advent of ultrashort extreme ultraviolet (XUV) pulses with subfemtosecond duration [1, 2], it has become possible to carry out time-resolved measurements of electronic dynamics in atoms and molecules. XUV-pump–XUV-probe experiments have been reported [3, 4], but they are still highly challenging because of the low intensities of the available XUV pulses. Therefore, many current experiments rely on pumping atoms or molecules by using subfemtosecond XUV pulses and probing the initiated dynamics with near-infrared (NIR) pulses. The first such XUV-pump–NIR-probe experiment was performed to measure the duration of an Auger decay in Kr atoms directly in the time domain using isolated attosecond pulses [5]. By analysing the photoelectron spectrum as a function of the time delay between the XUV pulse and the NIR pulse, a lifetime of about 8 fs was observed, in agreement with energy-domain spectra.

Over the last few years, the dynamical properties of Fano resonances caused by autoionization of metastable states have been investigated [6–9]. Doubly excited states lying above the one-electron ionization threshold are prime examples of autoionizing states. The doubly excited states can be viewed as discrete states embedded in the continuum. They decay into a free electron and an ion in the ground state, with the kinetic energy of the free electron determined by conservation of energy. This type of decay is a prototype process governed by the electron–electron interaction. One-photon absorption from the ground state into the energy range around a doubly excited state leads to ionization along two possible paths: either direct ionization into the background continuum or indirect ionization via the autoionizing resonance. The interference of the two paths gives rise to an asymmetric absorption line, which is known as the Fano profile [10]. The Fano profile is found in both photoelectron spectra and photoabsorption spectra. Indeed, in a few recent studies, the time-resolved autoionization dynamics has been investigated by analysing the laser-modified photoabsorption [11–13].

The helium atom is the simplest system that exhibits autoionization. For the XUV-pump–NIR-probe scheme, it has been shown that laser-induced ionization and laser-induced coupling between the doubly excited states 2s2p and $2p^2$ of helium play a crucial role in the autoionization process, leading to modification of the Fano resonance profile [13–15]. While the previous theoretical studies of time-resolved autoionization are based on the strong-field approximation or on few-level models, in this paper we approach the problem by numerical solution of the time-dependent two-electron Schrödinger equation (TDSE) for a one-dimensional (1D) helium model atom. The 1D atom exhibits a series of autoionizing states embedded in the single-ionization continuum [16]. The advantage of the 1D model is that the TDSE can be solved practically exactly with full account of the electron–electron interaction and without making assumptions about the dominant physical mechanisms. In our simulations, a single attosecond XUV pulse with broad bandwidth creates a wave packet consisting of several doubly excited states. The simultaneous XUV-induced population of different autoionizing states has been addressed only rarely in the literature [3, 7, 9, 17]. A time-delayed NIR laser pulse probes the autoionization dynamics. In this work, we focus on the photoelectron spectra. We demonstrate that the NIR-induced coupling between autoionizing states modifies the Fano profile and leads to additional peaks with asymmetric line profile in the photoelectron spectra. Modulations of these peaks upon variation of the time delay are found and explained. Interference effects due to the superposition of autoionizing states [7] are also observed. A fringe pattern that has been seen but not explained in previous theoretical studies [13] is

clearly observed in our results. It is determined by the time delay and is independent of the details of the laser pulse. We interpret this pattern as a consequence of the truncation of the autoionizing decay by the laser field.

Atomic units are used in this paper. For the presentation of the results, however, energies and times are given in units of eV and fs.

2. One-dimensional model

The two-electron TDSE for the 1D helium atom in the presence of an external field $E_{\rm ext}(t)$ reads

$$\mathrm{i}\,\partial_t \Psi(x_1, x_2, t) = \left[-\frac{\partial_1^2}{2} - \frac{\partial_2^2}{2} + V_0(x_1, x_2) + (x_1 + x_2) E_{\rm ext}(t)\right] \Psi(x_1, x_2, t) \tag{1}$$

with

$$V_0(x_1, x_2) = -\frac{2}{\sqrt{x_1^2 + 0.5}} - \frac{2}{\sqrt{x_2^2 + 0.5}} + \frac{1}{\sqrt{(x_1 - x_2)^2 + 0.339}}. \tag{2}$$

The soft-core parameters are chosen to reproduce the ground-state energies of 3D helium and the He^+ ion [18]. The wave function $\Psi(x_1, x_2, t)$ is represented on a numerical grid with a spatial step size of 0.5 au. Due to the discreteness of our grid, the calculated energy values of the autoionizing states may differ slightly by a few tenths of an eV from the exact values. This has negligible effect on the presented results.

The external field is a superposition of an XUV pulse $E_{\rm X}(t)$ and an NIR laser pulse $E_{\rm L}(t)$ linearly polarized in the same direction. We choose the frequencies $\omega_{\rm X} = 1.84\,\text{au} = 50.0\,\text{eV}$ and $\omega_{\rm L} = 0.038\,\text{au} = 1.03\,\text{eV}$ unless specified differently. The two pulses have the forms

$$E_{\rm X}(t) = E_{0\rm X} \exp\left(-(2\ln 2)\frac{t^2}{\tau_{\rm X}^2}\right) \cos(\omega_{\rm X} t) \tag{3}$$

and

$$E_{\rm L}(t) = E_{0\rm L} \cos^2\left(\frac{\pi(t - t_{\rm d})}{2.75\tau_{\rm L}}\right) \cos\left(\omega_{\rm L}(t - t_{\rm d}) + \phi\right), \quad |t - t_{\rm d}| < 1.373\tau_{\rm L}. \tag{4}$$

Here $E_{0\rm X}$ and $E_{0\rm L}$ are the electric-field amplitudes; $\tau_{\rm X}$ and $\tau_{\rm L}$ are the pulse durations defined as the full-width at half-maximum (FWHM) of the intensity envelope; ϕ is the carrier envelope phase (CEP) of the laser pulse and $t_{\rm d}$ is the time delay between the centres of the laser pulse and the XUV pulse. The sign of the delay is chosen such that for positive delays, the XUV pulse acts before the laser pulse.

The TDSE is solved by means of the split-operator technique [19] with 64 time steps per XUV cycle. The time evolution starts from the singlet ground state, which is obtained by imaginary-time propagation. Therefore the system is in a singlet state at all times, i.e. the wave function $\Psi(x_1, x_2, t)$ must be symmetric with respect to exchange of the electron position coordinates x_1 and x_2. Absorbing boundaries are employed but the grid is chosen large enough (at least 2000 au in each coordinate) to ensure that electrons will not reach the boundaries before the end of the pulses. We isolate the non-ground-state part $\bar{\Psi}(x_1, x_2, t_0)$ of the wave function at time t_0 after the pulses by projecting out the ground state. To obtain the photoelectron spectrum,

the wave function is then propagated further in time without external field until a final time t_f. From the time-dependent wave function, the autocorrelation function is calculated as

$$C(t) = \langle \bar{\Psi}(t_0) | \bar{\Psi}(t) \rangle. \tag{5}$$

The Fourier transform of the autocorrelation function yields the total energy spectrum

$$\sigma(E) = \frac{1}{\pi} \mathrm{Re} \int_{t_0}^{t_f} C(t)\, \mathrm{e}^{\mathrm{i}E(t-t_0)}\, \mathrm{d}t. \tag{6}$$

We use a long time interval $t_f - t_0 = 3420$ au for all calculations to guarantee sufficient energy resolution. Since autoionization of doubly excited states leaves the ion in the ground state, the kinetic energy E_f of the outgoing electron is determined by energy conservation, $E = E_f + E_g^+$, with E_g^+ being the ground-state energy of the singly charged ion.

The autocorrelation function is also used to obtain the energy levels of the unperturbed helium atom. Propagating from an arbitrary initial state yields the energies of the eigenstates contained in the initial state. Since the Hamiltonian is invariant under the parity operation ($x_1 \to -x_1$, $x_2 \to -x_2$), the nondegenerate eigenfunctions must satisfy the condition $\Psi(x_1, x_2) = \pm\Psi(-x_1, -x_2)$. To determine the parity of the eigenstates, we choose two different initial states. One is a Gaussian wave packet $\Psi_G(x_1, x_2) = \exp(-(x_1+4)^2/10 - (x_2+2)^2/10)$; the other is an even-parity wave packet $\Psi_s(x_1, x_2) = \sin(x_1)\sin(x_2)\exp(-x_1^2/10 - x_2^2/10)$, containing only eigenfunctions satisfying $\Psi(x_1, x_2) = \Psi(-x_1, -x_2)$.

3. Results and discussion

It is instructive to first present the energy level diagram of the 1D helium atom. The relevant levels are plotted in figure 1(a). Here we set the energy scale such that the ground-state energy equals 0. The notation $|n_1, n_2\rangle$ indicates that, in the limit of noninteracting electrons, one of the electrons is excited to state $|n_1\rangle$ of He^+ and the other is in the state $|n_2\rangle$. Here, $n = 1$ refers to the ground state, $n = 2$ to the first excited state and so on. The state $|2, 3\rangle$ at $E = 50.69$ eV is the lowest doubly excited state reachable by one-photon absorption from the ground state. The even-parity state $|2, 4\rangle$ is 0.75 eV above the state $|2, 3\rangle$ and the state $|2, 5\rangle$ is at $E = 52.41$ eV.

The energy spectrum after irradiation with an attosecond XUV pulse with FWHM $\tau_X = 171$ attoseconds is shown in the right panel of figure 1(a). The broad spectral distribution reflects the bandwidth of the XUV pump pulse. Due to the selection rules for electric dipole transitions, only the odd-parity states are populated by the attosecond XUV pulse. Therefore the doubly excited states $|2, 3\rangle$ and $|2, 5\rangle$ can be reached with one XUV photon, but not the states $|2, 2\rangle$ and $|2, 4\rangle$. The electron energy spectrum near a doubly excited state is given by the Beutler–Fano function [10]

$$P(E) = \frac{(q+\varepsilon)^2}{1+\varepsilon^2} \tag{7}$$

with the dimensionless reduced energy $\varepsilon = \frac{E-E_r}{\Gamma/2}$, which measures the energy relative to the resonance position E_r in units of $\Gamma/2$ where Γ is the width of the resonance. The Fano parameter q depends on the relative strength of the ionization via the doubly excited state compared to direct ionization into the background continuum. The Fano parameter determines the asymmetry of the Fano profile: for nonzero finite q, the line profile is asymmetric; for $|q| \to \infty$, a Lorentzian profile is recovered. The XUV-induced spectrum in figure 1(a)

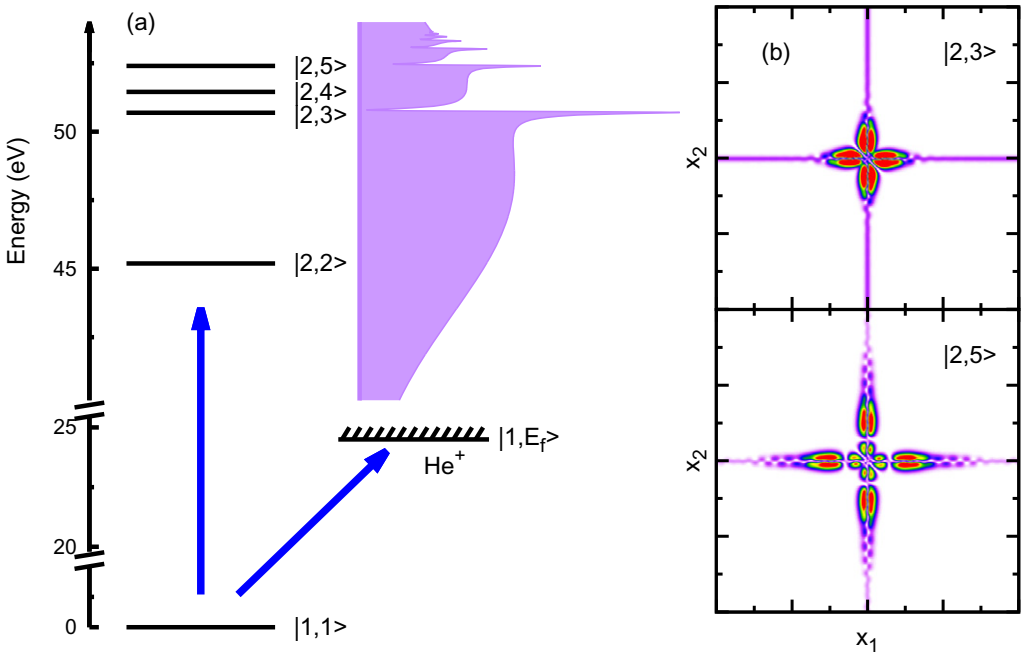

Figure 1. (a) Energy level diagram of the $|2, n\rangle$ autoionizing states in the 1D helium model and the energy spectrum after the action of a short XUV pulse. (b) Wave packets generated by excitation with long XUV pulses resonant with the states $|2, 3\rangle$ and $|2, 5\rangle$, respectively.

beautifully exhibits the typical asymmetric absorption lines. The largest weights are found for the states $|2, 3\rangle$ and $|2, 5\rangle$. By fitting the spectrum to the Beutler–Fano functions, the parameters of the resonance state $|2, 3\rangle$ are $E_r = 50.69\,\text{eV}$, $\Gamma = 0.086\,\text{eV}$ and $q = -1.21$; the parameters for the state $|2, 5\rangle$ are $E_r = 52.41\,\text{eV}$, $\Gamma = 0.054\,\text{eV}$ and $q = -1.17$. In comparison, the numbers for the well-known 2s2p resonance in the real helium atom are $E_r = 60.15\,\text{eV}$, $\Gamma = 0.037\,\text{eV}$ and $q = -2.75$ [20].

To obtain pictures of the doubly excited states, we excite the atom with longer XUV pulses such that only one of the states is covered by the bandwidth of the pulse. To select the $|2, 3\rangle$ or $|2, 5\rangle$ state, the XUV frequency is centred at 50.7 or 52.4 eV, respectively. The XUV pulse length (FWHM) is about 6.9 fs. By projecting out the two-electron ground state from the wave function after XUV irradiation, the two-electron wave packet containing the autoionizing state can be isolated. The modulus squared of the resulting wave functions is plotted in figure 1(b). The nodal structure is consistent with the single-particle excitations indicated by the quantum numbers. The wave function at large $|x_1|$ or large $|x_2|$ shows the transition of the quasi-bound state into an outgoing electron with the other electron bound in the nodeless single-electron ground state.

Returning to the case of attosecond XUV excitation (without probe laser pulse), we show in figure 2 the modulus squared of the two-electron wave packet (where the ground state has been projected out) at different times after the XUV pulse. The XUV parameters for these and the following simulations are: pulse length 171 attoseconds, central photon energy 50 eV and peak intensity $10^{12}\,\text{W cm}^{-2}$. At 5.13 fs after the XUV pulse, the inner-part wave packet resembles to some extent the autoionizing state $|2, 3\rangle$ in figure 1. However, the coherent superposition of

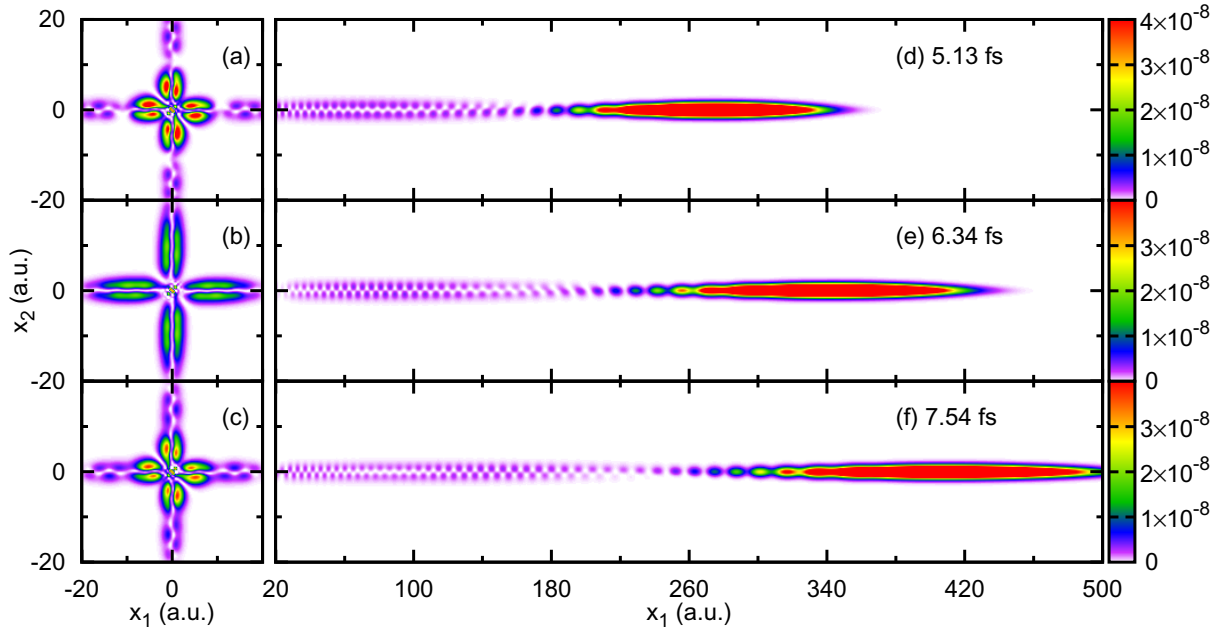

Figure 2. Left: modulus squared of the inner part of the two-electron wave packet after the XUV pulse, taken at different times. Right: modulus squared of the outer part of the wave function. The times in (a)–(c) are the same as in (d)–(f).

autoionizing states expresses itself in an oscillation of the quasi-bound wave packet in time. The period of this oscillation is expected to be $T = 2\pi/(E_{|2,5\rangle} - E_{|2,3\rangle}) = 2.41$ fs. The time evolution displayed in figures 2(a)–(c) clearly confirms the oscillation of the wave packet within the expected period. At the same time, the comparison of figures 2(a) and (c) shows the decrease of the overall population of the doubly excited states due to the decay.

The right panels of figure 2 show the wave function in the outer region. Obviously, the outgoing wave function consists of two parts. One is the broad continuous wave packet, plotted in red, representing direct ionization to the continuum. It escapes the core region immediately after excitation. The other part, lagging behind, represents an electron emerging by decay of autoionizing states. The coherent superposition of autoionizing states leads to interference in the outgoing waves. This interference gives rise to a hint of a slow oscillation along the x_1-axis. A spatial period of about 140 au matches the momentum difference between electrons from the states $|2, 3\rangle$ and $|2, 5\rangle$. The momenta of electrons from these two states are 1.389 and 1.434 au. The interference of these outgoing waves with quasi-bound Rydberg states (which can be thought of as extended momentum-zero states) leads to the fast oscillation with a spatial period of about 4.5 au.

In the following, we investigate in detail the probing of the autoionizing wave-packet dynamics by an NIR laser pulse. The laser peak intensity in these simulations is 2×10^{11} W cm^{-2} except for figure 3(d) where also the intensities 1×10^{11} and 5×10^{11} W cm^{-2} are used as indicated. We inspect the photoelectron spectrum around the $|2, 3\rangle$ absorption line for a variety of laser parameters. The energy axis in these plots gives the kinetic energy E_f of the outgoing electron. First, we compare different laser wavelengths for zero time delay between the XUV and NIR pulses, see figure 3(a). The frequencies 0.038, 0.040 and 0.046 au correspond

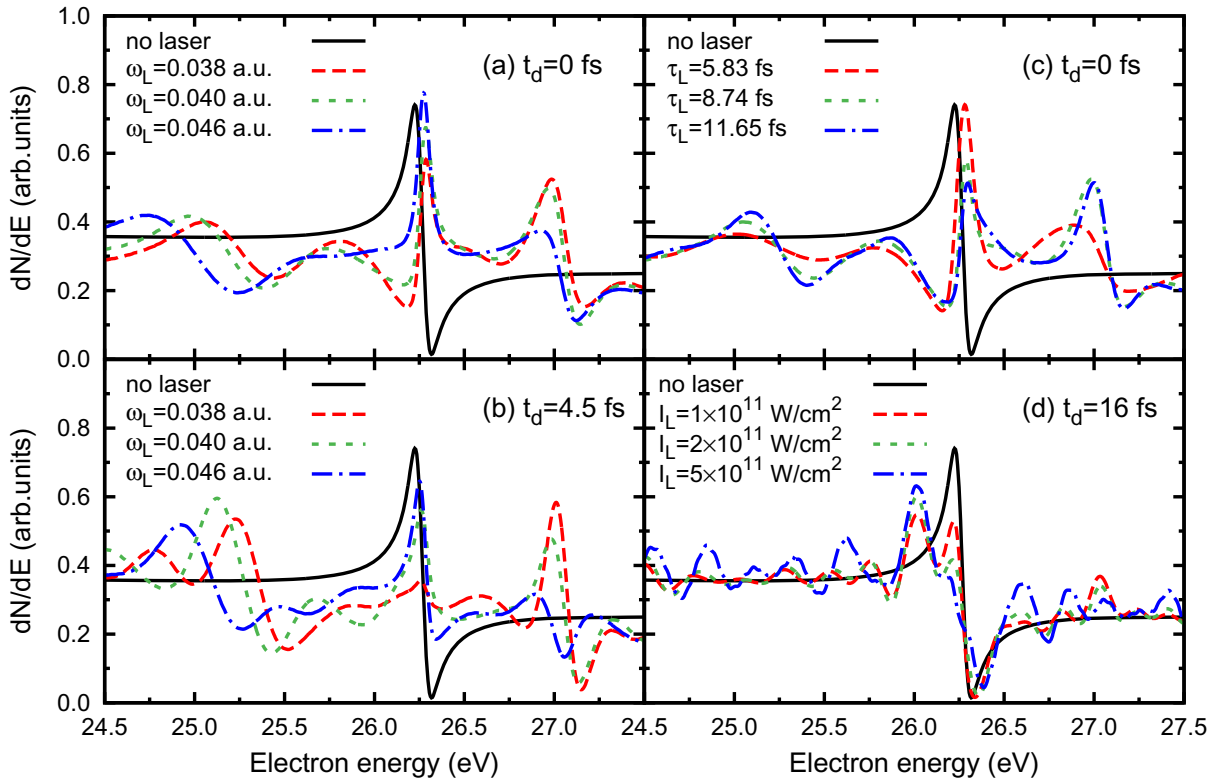

Figure 3. (a) Photoelectron spectra for different laser frequencies ω_L at time delay zero. (b) The same as (a) for the time delay of 4.5 fs. (c) Photoelectron spectra with different laser pulse lengths. The frequency is $\omega_L = 0.038$ au. (d) Photoelectron spectra for various laser intensities at time delay 16 fs (no overlap between XUV and laser pulses). The laser pulse lengths in (a), (b) and (d) are $\tau_L = 8.74$ fs for $\omega_L = 0.038$ au, $\tau_L = 8.30$ fs for $\omega_L = 0.040$ au and $\tau_L = 7.22$ fs for $\omega_L = 0.046$ au.

to the wavelengths 1.20, 1.14 and 0.99 μm. It is apparent that the Fano profile at 26.26 eV is strongly modified by the laser field. Additionally, electrons with energies around 27 eV appear in the presence of the laser pulse. The position of this peak is found to be independent of the laser wavelength and coincides with the $|2, 4\rangle$ doubly excited state. The explanation is that the NIR laser field couples states of opposite parity. In a quasi-static picture, the instantaneous laser field dresses the doubly excited states and breaks the inversion symmetry, so that XUV absorption to the dressed states need not respect the laser-free selection rules. When the laser field ends, population remains in the $|2, 4\rangle$ state and decays by autoionization. This process is found to become less efficient with increasing laser frequency. The line shape is obviously asymmetric. This shows that the autoionization of the $|2, 4\rangle$ state interferes with the direct ionization path.

Similar effects take place for the delay $t_d = 4.5$ fs as shown in figure 3(b). At this delay, we observe another characteristic feature of the XUV-pump–NIR-probe scheme, namely the appearance of a sideband: the peaks around 25 eV in figure 3(b) are one laser photon below the $|2, 3\rangle$ resonance. For $t_d = 0$ (figure 3(a)), the sideband is present as well, but it is less clear. A sideband could in principle exist also on the high-energy side of the resonance; it seems to be suppressed by the presence of the state $|2, 4\rangle$ in the same energy region. Sidebands have been

seen clearly in the XUV-pump–NIR-probe photoelectron spectra from helium [8]. Sideband intensities have been exploited to deduce the Auger lifetime of a Kr inner-shell excitation in [5], since the sideband can be created only during the lifetime of the populated metastable state. As discussed in [7], the lifetime of a Fano resonance can also be read from the decay of the sideband for nonoverlapping XUV and laser pulses.

The photoelectron spectra for different laser pulse lengths are shown in figure 3(c). With increasing pulse length, there is more time available to form the sideband. At the same time, the central Fano profile is depleted. The population of the state $|2, 4\rangle$ around 27 eV, however, is hardly increased by increasing the pulse length above 8.74 fs. This is in accordance with the physical interpretation that the population transfer to the $|2, 4\rangle$ state is mainly achieved during the XUV pulse. Figure 3(c) clearly shows the modification of the Fano line shape at 26.26 eV. We find an inverse Fano line, which has been discussed earlier in [15].

At a larger time delay of 16 fs, the XUV and NIR pulses do not overlap in time any more. At this delay, the autoionizing states have substantially decayed so that the laser-assisted transfer of electrons to the sideband or to the $|2, 4\rangle$ state is weak. The Fano profile, on the other hand, is strongly changed as compared with the laser-free profile. The spectrum is dominated by a side peak at 25.9 eV. Since the position of this peak is insensitive to the laser intensity (see figure), we do not interpret it in terms of the Autler–Townes splitting [11, 21, 22]. Similar structures have been seen in the calculations of [13, 15] where they were explained as a superposition of the regular and an inverse Fano profile. Below we give a different interpretation.

The photoelectron spectra as a function of time delay are shown in figure 4. The laser parameters in this simulation are: peak intensity $2 \times 10^{11}\,\mathrm{W\,cm^{-2}}$, frequency 0.038 au, pulse lengths 5.83 fs in (a) and (b) and 8.74 fs in (c). In each panel, the small red curve is a picture of the respective total electric field versus time for the delay $t_\mathrm{d} = 0$.

In the region of large negative delays, see for example figures 4(a) and (b), from −8 to −4 fs, the laser pulse arrives before the XUV pulse and only the tail of the laser pulse is involved in the dynamics. Therefore, the spectrum is similar to the XUV-only case. For overlapping XUV and laser pulses, complex behaviour of the spectrum is found. The efficiency of populating the $|2, 4\rangle$ state at 27 eV oscillates as a function of delay with about half the period of the NIR field. This is most clearly seen in the case of the longer laser pulse, see figure 4(c). In this case, the population in $|2, 4\rangle$ is large when the XUV pulse arrives close to the centre of the laser pulse or at a time of maximum of the laser field in the range $t_\mathrm{d} > 0$. This shows that the population is sensitive to the instantaneous electric field. In the simulation for a CEP of $\pi/2$ shown in figure 4(b), the oscillation in the $|2, 4\rangle$ peak is accordingly phase-shifted with respect to the case of zero CEP in figure 4(a). We attribute the deviations from an exact half-cycle modulation to the rapidly varying envelope of the few-cycle laser pulses. It is interesting to note that the main Fano profile at the $|2, 3\rangle$ state tends to be inverted at times of maximum population in $|2, 4\rangle$. The sideband around 25 eV oscillates as a function of the time delay as well. Its maxima appear at the same times as the maxima of the $|2, 4\rangle$ state. This is again most clearly seen for the interaction with the longer laser pulse in figure 4(c).

In the following we discuss the region where the laser pulse arrives after the XUV pulse without overlap. This is the case for time delays longer than 8 fs in figure 4(a). Apparently, the main Fano line at the $|2, 3\rangle$ state is strongly depleted. We see a characteristic curved fringe pattern on the low-energy side and to a lesser extent on the high-energy side. Similar patterns have been found already in the previous theoretical studies in [13], but they have not been explained. It is one of these fringes that gives rise to the side peak in figure 3(d). Its position

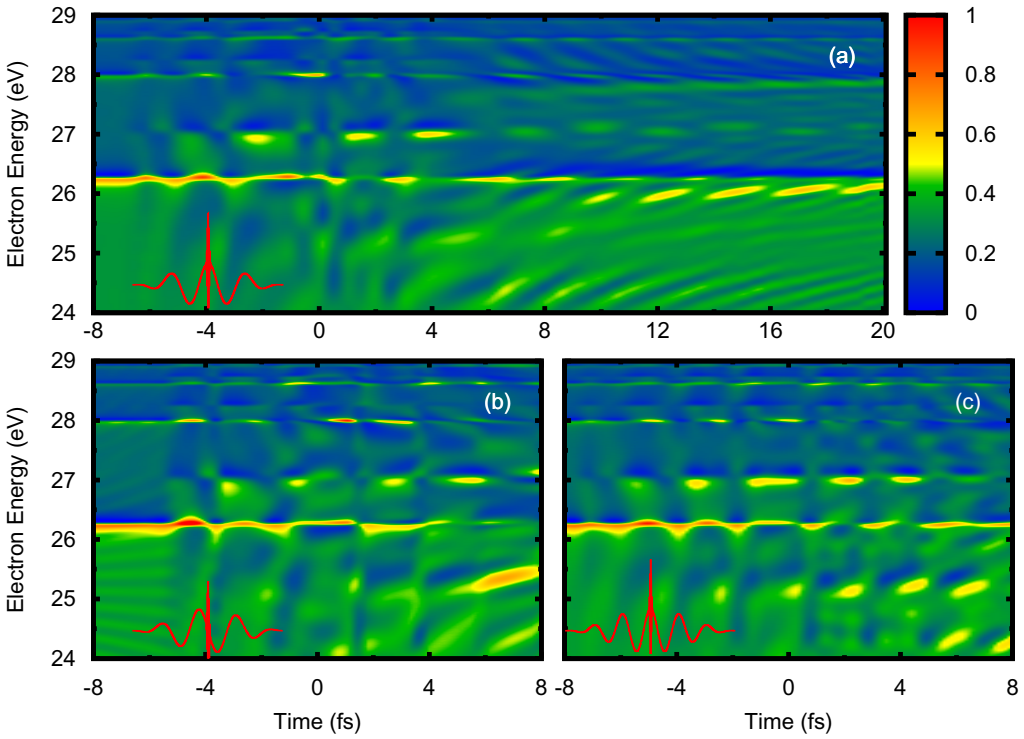

Figure 4. Photoelectron spectra as a function of time delay between the NIR and XUV pulses. (a) Laser pulse length $\tau_L = 5.83$ fs, CEP $\phi = 0$. (b) Laser pulse length $\tau_L = 5.83$ fs, CEP $\phi = \pi/2$. (c) Laser pulse length $\tau_L = 8.74$ fs, CEP $\phi = 0$. The laser frequency is $\omega_L = 0.038$ au. To illustrate the XUV and NIR fields, the red curves show the total electric field versus time on an arbitrary scale for time delay zero.

is independent of the laser intensity. Our results indicate that the overall pattern is not very sensitive to the laser pulse parameters. Instead, the fringes follow curves where the product $|E - E_r|t_d$ is constant with E_r being one of the resonance energies. For large delays, these fringes converge to the resonance energy. For example, the line between 27.5 and 27.8 eV at times $t_d > 6$ fs approaches the $|2, 5\rangle$ resonance at 27.98 eV from below. We can understand the appearance of these fringes as a consequence of a truncated decay of a metastable state. If an exponentially decaying amplitude of the form $\exp(-iE_r t - \Gamma t/2)$ is Fourier transformed to the energy domain using as an upper limit not infinite time but a finite time t_d, one will encounter terms proportional to $\cos((E - E_r)t_d)$ where E is the energy variable and E_r is the resonance energy. Hence, we expect that the condition for obtaining maximum or minimum signal follows curves satisfying $|E - E_r|t_d = n\pi$ with integer n. This is confirmed by figure 4. It is natural to assume that the action of the time-delayed laser pulse can truncate the exponential decay, for example by sudden ionization of the atom, see figure 3(a) of [11] for an illustration. We may even speculate that the laser-induced line shifts of the autoionizing argon states measured in the experiment [11] are not due to an Autler–Townes-type splitting, but that they obey a fringe pattern law as described above. When the fringes are superimposed with the regular Fano profile (due to autoionizing decay after the NIR pulse in the case when the doubly excited state has not been entirely emptied), a hybrid structure is formed as in figure 3(d) for the lowest laser intensity.

Although our interpretation agrees with [15] to the extent that the overall spectrum is formed by overlaying the contributions from before and after the laser pulse, our understanding of the pre-laser-pulse contribution is a different one. The detailed analysis and modelling of the fringes will be a subject of future work. Similar delay-dependent fringes due to interference between laser-induced ionization from XUV-populated bound excited states and direct ionization by XUV absorption have been discussed in [23].

Another interesting feature at long time delay in figure 4(a) is the modulation of the peak near 26 eV, just below the $|2, 3\rangle$ resonance at 26.26 eV. It can be easily verified that the oscillation as a function of delay has a period of about 2.4 fs, in agreement with the energy gap between the states $|2, 3\rangle$ and $|2, 5\rangle$. This type of oscillation for coherent excitation of two resonances has already been pointed out in [7] and measured experimentally [9]. It corresponds to the quasi-periodic motion apparent in the coordinate-space plots in figures 2(a)–(c). The same oscillation period is found in the population of the $|2, 4\rangle$ state at 27 eV in the photoelectron spectrum for long delay. Closer inspection of these structures reveals that they exhibit also a slight modulation to higher and lower energies as the delay is varied. The period, however, is given by the energy gap between the states $|2, 3\rangle$ and $|2, 4\rangle$. If we interpret the small energy shifts as the signature of an asymmetric line shape, it is easily understood that the sign of asymmetry depends on the relative phase between the background continuum and the electrons from the autoionizing $|2, 4\rangle$ state. This relative phase must include the phase that the electrons have acquired in the $|2, 3\rangle$ state before being transferred by the laser field to the $|2, 4\rangle$ state. Thus, the sign of the Fano profile can simply be controlled by applying the laser pulse at a certain time delay.

4. Conclusion

Autoionization dynamics of 1D helium has been investigated by numerical solution of the TDSE. An autoionizing wave packet is excited by an attosecond XUV pulse and probed by a time-delayed NIR laser pulse. Besides confirming previously known effects such as sideband formation and laser-induced coupling between autoionizing states, we have gained new insight into the laser-induced line shifts. The truncation of the autoionizing decay by the NIR field forms a universal fringe pattern in the photoelectron spectra. The peaks arising from the laser-induced coupling between states are modulated with time delay. This means that control of Fano line shapes is possible by suitable timing of an NIR pulse.

Acknowledgments

We thank the Deutsche Forschungsgemeinschaft for funding the Centre for Quantum Engineering and Space-Time Research (QUEST). JZ acknowledges support from the China Scholarship Council and discussions with Zengxiu Zhao.

References

[1] Hentschel M, Kienberger R, Spielmann C, Reider G A, Milosevic N, Brabec T, Corkum P, Heinzmann U, Drescher M and Krausz F 2001 *Nature* **414** 509–13

[2] Paul P M, Toma E S, Breger P, Mullot G, Augé F, Balcou P, Muller H G and Agostini P 2001 *Science* **292** 1689–92

[3] Skantzakis E, Tzallas P, Kruse J E, Kalpouzos C, Faucher O, Tsakiris G D and Charalambidis D 2010 *Phys. Rev. Lett.* **105** 043902
[4] Tzallas P, Skantzakis E, Nikolopoulos L A A, Tsakiris G D and Charalambidis D 2011 *Nature Phys.* **7** 781–4
[5] Drescher M, Hentschel M, Kienberger R, Uiberacker M, Yakovlev V, Scrinzi A, Westerwalbesloh T, Kleineberg U, Heinzmann U and Krausz F 2002 *Nature* **419** 803–7
[6] Wickenhauser M, Burgdörfer J, Krausz F and Drescher M 2005 *Phys. Rev. Lett.* **94** 023002
[7] Zhao Z X and Lin C D 2005 *Phys. Rev.* A **71** 060702
[8] Gilbertson S, Chini M, Feng X M, Khan S, Wu Y and Chang Z 2010 *Phys. Rev. Lett.* **105** 263003
[9] Geiseler H, Rottke H, Zhavoronkov N and Sandner W 2012 *Phys. Rev. Lett.* **108** 123601
[10] Fano U 1961 *Phys. Rev.* **124** 1866–78
[11] Wang H, Chini M, Chen S, Zhang C H, He F, Cheng Y, Wu Y, Thumm U and Chang Z 2010 *Phys. Rev. Lett.* **105** 143002
[12] Gaarde M B, Buth C, Tate J L and Schafer K J 2011 *Phys. Rev.* A **83** 013419
[13] Chu W C and Lin C D 2012 *Phys. Rev.* A **85** 013409
[14] Loh Z H, Greene C H and Leone S R 2008 *Chem. Phys.* **350** 7–13
[15] Chu W C, Zhao S F and Lin C D 2011 *Phys. Rev.* A **84** 033426
[16] Haan S L, Grobe R and Eberly J H 1994 *Phys. Rev.* A **50** 378–91
[17] Wickenhauser M, Burgdörfer J, Krausz F and Drescher M 2006 *J. Mod. Opt.* **53** 247–57
[18] Li P C, Zhou X X, Wang G L and Zhao Z X 2009 *Phys. Rev.* A **80** 053825
[19] Feit M, Fleck J Jr and Steiger A 1982 *J. Comput. Phys.* **47** 412–33
[20] Domke M, Schulz K, Remmers G, Kaindl G and Wintgen D 1996 *Phys. Rev.* A **53** 1424–38
[21] Autler S H and Townes C H 1955 *Phys. Rev.* **100** 703–22
[22] Lambropoulos P and Zoller P 1981 *Phys. Rev.* A **24** 379–97
[23] Mauritsson J *et al* 2010 *Phys. Rev. Lett.* **105** 053001